J Mater Sci (2013) 48:4461–4466
DOI 10.1007/s10853-013-7155-6

NANOSTRUCTURED MATERIALS

Recent developments in modelling of microhardness saturation during SPD processing of metals and alloys

Alexander P. Zhilyaev · Azat A. Gimazov · Terence G. Langdon

Received: 30 October 2012 / Accepted: 10 January 2013 / Published online: 26 January 2013

Abstract Ultrafine-grained and even nanostructured materials can be fabricated using severe plastic deformation to ultra-high strains in equal-channel angular pressing (ECAP), high-pressure torsion (HPT), machining and their combinations, such as machining of ECAP specimens, HPT of ECAP billets and HPT of machining chips. This report presents recent results of investigations of the microstructures and microtextures of pure copper, nickel and aluminium subjected to different deformation processes to ultimately high imposed strains. A comparison of the microstructure, dislocation density and microhardness developed during combinations of different strain paths is performed. All characteristics were analysed by X-ray, transmission and scanning electron microscopy, and electron backscatter diffraction (EBSD). The influence of different processing routes is discussed in terms of the accumulated strain and microstructure refinement. The saturation in grain refinement is examined with reference to the recovery taking place during ultra-high strain deformation. A phenomenological model based on the Voce equation is applied for fitting parameters based on the experimental data and this is suggested for a prediction of microhardness evolution for pure metals (Ag, Au) and Cu-based (Zn, Al) alloys.

A. P. Zhilyaev · T. G. Langdon
Materials Research Group, Faculty of Engineering and the Environment, University of Southampton, Southampton SO17 1BJ, UK

A. P. Zhilyaev (✉) · A. A. Gimazov
Institute for Metals Superplasticity Problems, Russian Academy of Science, 39 Khalturina, Ufa 450001, Russia
e-mail: a.zhilyaev@soton.ac.uk

T. G. Langdon
Departments of Aerospace & Mechanical Engineering and Materials Science, University of Southern California, Los Angeles, CA 90089-1453, USA

Introduction

Ultrafine-grained materials obtained by severe plastic deformation (SPD) are attracting substantial interest because of their improved mechanical and physical properties [1–5]. However, the properties of these materials at the submicrometre and nanometre scale are not easily predicted from the behaviour observed in their coarse-grained counterparts. These difficulties arise primarily because the characteristic length of many physical processes (e.g. diffusion, heat transfer, charge carrier transfer etc.) may become comparable with the grain size and also there may be a predominance of interfacial phenomena and the emergence of new physical processes [6].

During monotonic (and quasi-monotonic such as ECAP) processing there appears to be a saturation in the grain refinement which is not at present understood. Furthermore, the situation is complicated because there have been numerous attempts to combine different processes routes [7, 8]. Indeed, the different processing routes of ECAP were used for a similar purpose and it was shown that route B_C of ECAP is most efficient for promoting a refined and equiaxed grain structure [9]. Recent reports considered the potential for improving the properties of materials by introducing straining by high-pressure torsion (HPT) of electrodeposited nickel [10], hot-compaction of ball milled Al–Pb alloy [11] and consolidation by HPT of Al–W alloys after ball milling [12]. It may be anticipated that an abrupt change in the processing route may lead to a greater refinement of the microstructure.

This report examines recent results from investigations of the microstructures and microtextures of pure copper, nickel

and aluminium subjected to different deformation processes to high ultimate imposed strains. A comparison of microstructure, dislocation density and microhardness developed during combinations of different strain paths is performed. All characteristics are analysed by X-ray, transmission and scanning electron microscopy, and electron backscatter diffraction (EBSD). The influence of different processing routes is discussed in terms of the accumulated strain and microstructure refinement. A phenomenological model based on the Voce equation is applied for fitting parameters on basis of the experimental data and this was used for a prediction of microhardness evolution for pure metals (Ag, Au) and Cu-based (Zn, Al) alloys.

Experimental materials and procedures

Commercially pure copper, nickel and aluminium were processed at room temperature by equal-channel angular pressing (ECAP) for 4 (Cu, Al) or 8 (Ni) passes by route B_C using a 90° die [13]. High-pressure torsion discs were processed at room temperature, under an applied load of $P = 6.0$ GPa for five complete revolutions. Additional nickel samples were processed by unconstrained HPT for totals of $N = 5$, 10 or 20 turns under an applied pressure of $P = 6.0$ GPa [8]. Subsequently, the ECAP billets were machined (in this paper the process of machining is designated as M) into chips and they were placed in the depression on the lower anvil of a constrained HPT facility and consolidated at room temperature under the same conditions of $P = 6.0$ GPa and $N = 5$ turns. HPT discs of copper, nickel and aluminium prepared from the machined chips were essentially fully dense and there was no evidence of any visible cracking. All consolidated discs were 10 mm in diameter and approximately 0.2–0.5 mm in thickness. These discs were mechanically polished to a mirror-like finish for microhardness testing using a load of 0.1 kg and a holding time of 10 s. Details of the specimen preparation for TEM and EBSD analyses can be found elsewhere [7, 8, 14–18]. The TEM foils were cut from the half-radius positions in the discs and X-ray analysis was performed on these foils prior to electropolishing. For X-ray diffraction (XRD), the coherent domain size and the microstrain were determined using appropriate XRD data analysis software (materials analysis using diffraction (MAUD) [19]) based on the full pattern fitting or Rietveld method [20].

Experimental results

All data for highly strained pure metals are summarised in Table 1 (Cu), Table 2 (Ni) and Table 3 (Al). This order is listed according to the stacking fault energy (SFE) [21] of copper (78 mJ/m^2), nickel (125 mJ/m^2) and aluminium (166 mJ/m^2). The first row in the Tables indicates the routes of processing, where these routes are either single (ECAP or HPT) or combined (e.g. ECAP+HPT). The second row corresponds to the equivalent strain accumulated, calculated by the Hencky strain for consequent routines and summed on the basis of an additive law. The third row shows the microhardness level of materials measured for different conditions. The fourth and fifth rows specify the crystallite size and level of dislocation density evaluated on the basis of X-ray analysis. Finally, the sixth and seventh rows show the mean grain sizes obtained from TEM and EBSD measurements, respectively.

As can be seen from the Tables, all pure metals having different stacking fault energies tend to become saturated in microhardness, grain size and dislocation density. However, although for aluminium (lowest melting point, highest SFE) and copper (medium melting point, lowest SFE) the saturation is evident, for nickel (highest melting point, medium SFE) it is not so obvious. This observation is supported by TEM and EBSD structures shown in Figs. 1, 2 and 3. Examples of the microstructure, microtexture and 111 pole figures for copper, and nickel processed to high-strained conditions by ECAP, machining and the subsequent HPT consolidation of machined chips are represented in Figs. 1 and 2. The microstructure of ECAP+M+HPT copper consists of a bimodal grain structure indicating that there is some recovery during the consolidation/deformation process. The mean grain size by TEM (Fig. 1a) is about 210 nm and that is very close to the mean grain size (area weighted) of 220 nm by EBSD (Fig. 1b). In the colour-coded map of the ECAP+M+HPT copper, it is noted that some large grains appear in the grain structure. The 111 pole figure (Fig. 1c) reflects a shear texture (as it appears from the top plane). In all pole figures, RD corresponds to radial direction and TD is a tangential direction of the HPT disc. The intensity maxima have 2.66 × random levels. Similar microstructural characteristics are present in highly strained nickel processed by the same routines (ECAP, machining and HPT). The mean grain size in the nickel sample is about 100 nm by TEM (Fig. 2a) and it is significantly smaller than measured by EBSD (Fig. 2b) where the area weighted grain size is about 280 nm. It is noteworthy that this is the mean size of grains delineated by high-angle boundaries having misorientation angles $> 15°$. In practise, it is apparent that some of the larger grains have colour gradients which indicate the presence of a substructure and this will contribute to the grain size when measured in the TEM micrographs. The 111 pole figure (Fig. 2c) shows a slightly stronger texture (2.89 × random) developed in nickel after ECAP+M+HPT processing.

Figure 3 illustrates the TEM and EBSD microstructures in aluminium processed by HPT ($P = 6.0$ GPa, $N = 5$ turns). The mean grain sizes detected by both methods

Table 1 Microstructure parameters of highly strained copper [7, 22, 33]

Parameters	Initial	M	ECAP	ECAP+M	HPT	M+HPT	ECAP+HPT	ECAP+M+HPT
Accumulated strain	0	1.02	2.40	3.42	5.83	6.85	8.23	9.25
Microhardness (GPa)	1.03	1.45	1.40	1.57	1.72	1.73	1.71	1.94
Mean grain size, nm (XRD)	49	10	22	9	17	13	14	13
Dislocation density, 10^{14}, m^{-2}	0.15	1.93	1.66	2.29	0.48	0.56	0.57	0.55
Mean grain size, μm (TEM)	>5	–	0.5	–	0.32	0.31	0.31	0.21
Mean grain size, μm (EBSD)	–	–	–	–	0.26	0.24	0.27	0.22

Table 2 Microstructure parameters of highly strained nickel [8, 14, 15]

Parameters	Initial	ECAP	ECAP+CR	HPT	HPT (10)	HPT (20)	ECAP+HPT	ECAP+CR+HPT
Accumulated strain	0	3.21	3.92	5.83	6.64	7.44	9.04	9.25
Microhardness (GPa)	0.64	2.60	–	2.73	3.08	3.12	3.20	3.30
Mean grain size, nm (XRD)	–	29	25	26	26	22	24	15
Dislocation density, 10^{14}, m^{-2}	–	9	11	17	30	57	25	20
Mean grain size, μm (TEM)	–	0.35	0.30	0.17	0.15	0.08	0.14	0.10
Mean grain size, μm (EBSD)	–	–	–	–	–	–	–	0.28

Table 3 Microstructure parameters of highly strained aluminium [16–18, 33]

Parameters	Initial	M	ECAP	ECAP+M	HPT	M+HPT	ECAP+HPT	ECAP+M+HPT
Accumulated strain	0	1.02	2.40	3.42	5.83	6.85	8.23	9.25
Microhardness (GPa)	0.32	0.56	0.57	0.68	0.74	0.69	0.75	0.76
Mean grain size, μm (XRD)	0.91	0.37	0.31	0.28	0.37	0.32	0.34	0.27
Dislocation density, 10^{14}, $м^{-2}$	1.92	6.35	7.07	8.49	3.46	3.57	3.31	3.63
Mean grain size, μm (TEM)	–	–	1.2	–	0.8	–	–	–
Mean grain size, μm (EBSD)	33.5	–	–	–	0.9	–	–	–

were quite close with values of 0.8 μm by TEM and 0.9 μm by EBSD. This similarity indicates that there is substantial recovery and even recrystallization during SPD processing and this leads to a highly misoriented grain structure. Additional evidence for recovery is the strength and type of texture (Fig. 3c) formed in HPT aluminium: thus, it is stronger than in Cu and Ni and there is evidence for a recrystallization texture [22].

From the results described above, it seems that a refined substructure develops in the earlier stage of SPD processing and continued straining leads to a transformation from a subgrain structure to a grain structure with highly misoriented grain boundaries.

Discussion

There are several reports describing models of saturation in grain refinement during SPD processing for materials having different SFE [3, 21, 23]. Much attention has been given to the Cu-based (Zn, Al) alloys in which a decrease in the SFE by increasing alloying content produces higher microhardness and a finer grain structure [24–28]. In those reports, it was concluded that the SFE plays a major role in the grain refinement ability of these materials: thus, with decreasing SFE the minimum achievable grain size decreases and the microhardness increases.

However, there are two additional factors influencing grain refinement: (i) the melting point of the material and (ii) the alloying content. Recently, significant softening and grain growth were reported during HPT of the Cu-30 % Zn alloy [29] and this was attributed to the decomposition of the supersaturated solution during straining. In this sense, pure metals (such as Al, Ni and Cu) with different SFE can be used to evaluate the role of SFE in grain refining. However, the second factor of different melting temperatures can make this analysis more complex. Nevertheless, a phenomenological model may be proposed that takes into account the different melting points.

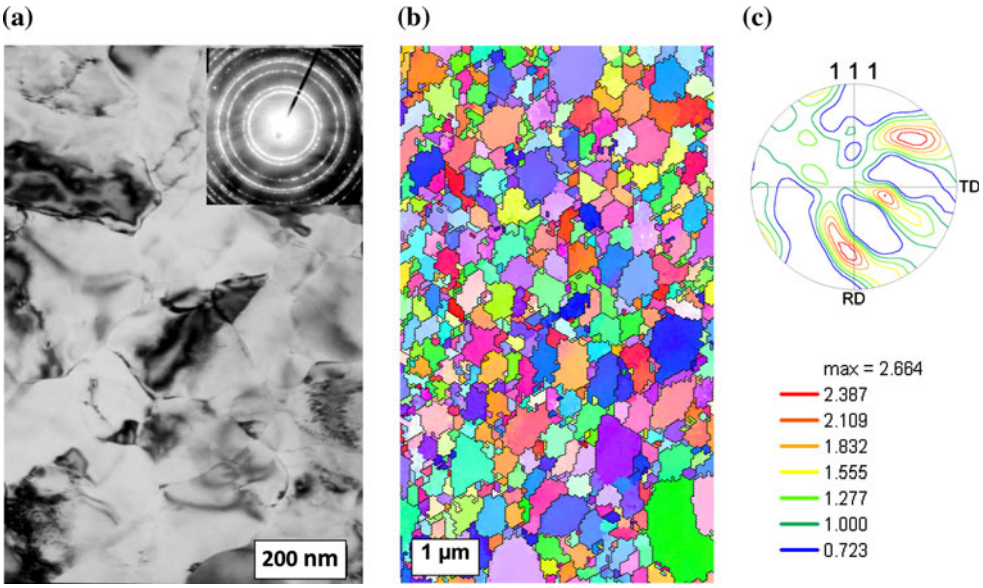

Fig. 1 Microstructure and microtexture of ECAP+M+HPT copper: **a** TEM; **b** EBSD; **c** 111 pole figure. RD corresponds to radial direction and TD is a tangential direction of the HPT disc

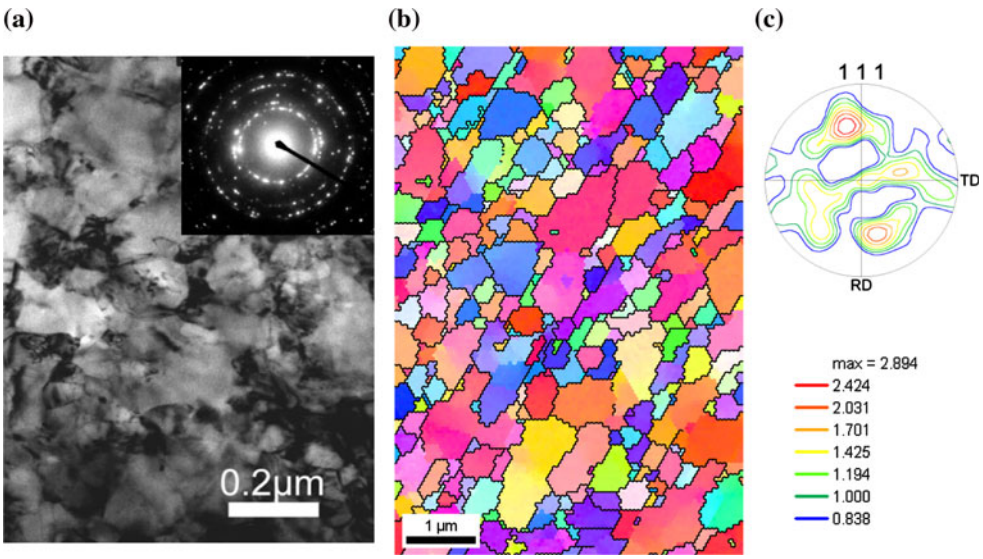

Fig. 2 Microstructure and microtexture of ECAP+M+HPT nickel: **a** TEM; **b** EBSD; **c** 111 pole figure. RD corresponds to radial direction and TD is a tangential direction of the HPT disc

In earlier reports [30, 31] it was proposed to use the Voce relation [32] for microhardness, H_V, where,

$$H_V = H_{V0} + A \cdot (1 - exp(-n \cdot \varepsilon)) \quad (1)$$

where H_V is the microhardness as a function of the accumulated strain, ε, H_{V0} is the initial microhardness and A and n are fitting parameters. Applying a fitting procedure for curves of Al, Ni and Cu, it is possible to obtain fitting parameters A and n for each metal as listed in Table 4, where A depends on some material parameters such as the shear strength or melting temperature. Plotting A as a function of the melting temperature, $A = f(T_m/T - 1)$, for aluminium, nickel and copper, it follows that the parameter A can be fitted to a polynomial in Fig. 4a which is of the form:

$$A = 0.091(\mp 0.007) \cdot \left(\frac{T_m}{T} - 1\right)^2 + 0.0069(\mp 0.0008) \cdot \left(\frac{T_m}{T} - 1\right) \quad (2)$$

The parameter n plotted as a function of the stacking fault energy, γ_{SF}, in Fig. 4b shows that there is a linear dependence on the SFE given by:

$$n = 1.706(\mp 0.029) + 5.964(\mp 0.225) \cdot \gamma_{SF} \quad (3)$$

This is confirmation of the validity of this procedure because for many metallic materials the strain hardening exponent of the Hollomon relation, which seems to be valid for strains less than 1, follows the same trend: it decreases with increasing SFE. Using Eqs. (2) and (3), it is

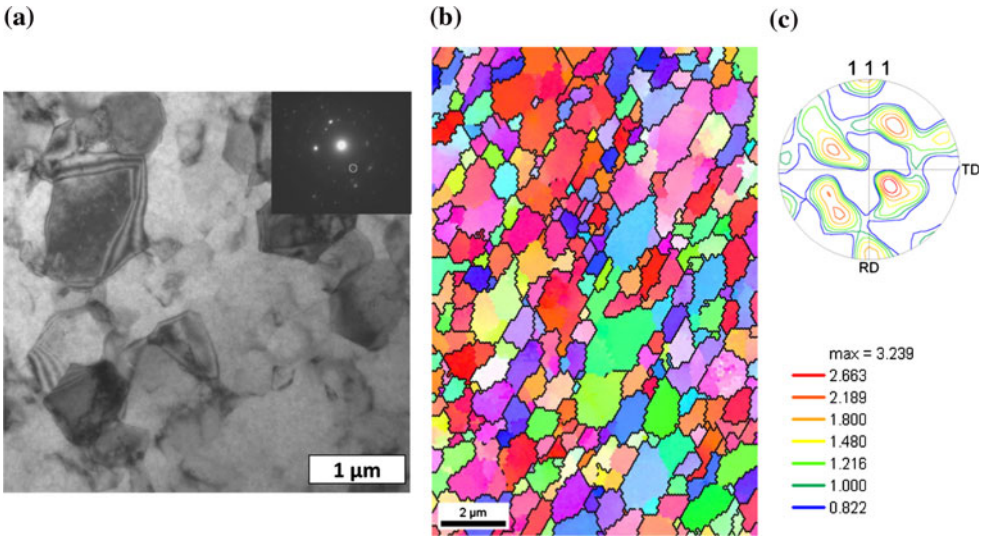

Fig. 3 Microstrcture and microtexture of HPT ($P = 6$ GPa, $N = 5$) aluminium: **a** TEM; **b** EBSD; **c** 111 pole figure. RD corresponds to radial direction and TD is a tangential direction of the HPT disc

Table 4 Stacking fault energy, melting point and fitted parameters for Al, Ni and Cu

Metals	T_m (K)	SFE (mJ/m^2)	A (GPa)	n
Aluminium	933	166	0.562	0.78
Nickel	1728	125	2.420	0.85
Copper	1357	78	0.134	1.29

possible to calculate $H_V - H_{V0}$ as a function of accumulated strain not only for Al, Ni and Cu but also for other fcc metals (e.g. silver and gold). Figure 5a depicts the calculated microhardness based on Eqs. (1) through (3) for aluminium, nickel, copper, silver and gold. In real experiments the order of the curves may change depending on the initial microhardness. Nevertheless, all curves show the saturation in microhardness as expected using a Voce-type fitting function. In practise, the experimental data shown by symbols in Fig. 5a for copper and nickel lead to a saturation with increasing strain. Inspection shows that this trend is less pronounced for copper which may be explained by experimental error but for nickel it is apparent from Fig. 5a that the strain hardening is still not saturated.

Using Eqs. (2) and (3) obtained for pure metals, it is possible to calculate the microhardness evolution for Cu-based (Zn, Al) alloys which have a strong dependence of grain refinement on the SFE. The melting temperatures, values of the SFE and the parameters A and n are given in Table 5 and the corresponding values of H_V–H_{V0} are shown in Fig. 5b as a function of strain. Again, the order of the microhardness curves depends on the initial microhardness and may not coincide with the observations in experiments. Surprisingly, the model predicts an H_V level for the Cu-30 % Zn alloy which is below the curves of the remaining alloys. Additionally, all curves are below the microhardness of pure copper in accordance with the melting temperature. It may be concluded, therefore, that the alloying content plays a significant role in strain hardening during SPD processing of these alloys.

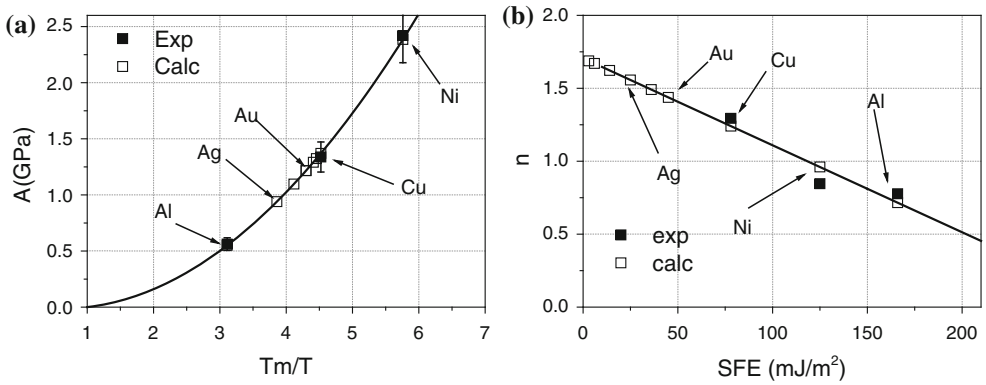

Fig. 4 Fitting parameters: **a** A as a function of melting point; **b** n as a function of stacking fault energy. *Open symbols* are calculated parameters, A and n, for Cu-based (Zn, Al) alloys

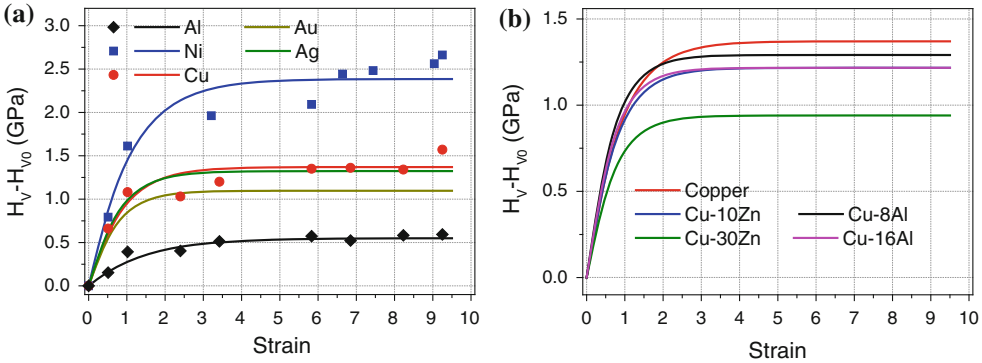

Fig. 5 Predicted strain hardening H_V–H_{V0} of metals and alloys with different stacking fault energy as a function of strain for: **a** pure metals (symbols are experimental points); **b** Cu-based (Zn, Al) alloys

Table 5 Stacking fault energy, melting point and fitted parameters for Cu and Cu-based (Zn, Al)-alloys

Metals	T_m (K)	SFE (mJ/m^2)	A (GPa)	n
Copper	1357	78	0.134	1.29
Cu-10 %Zn	1290	36	1.220	1.49
Cu-30 %Zn	1158	14	0.940	1.62
Cu-8 %Al	1323	6	1.290	1.67
Cu-16 %Al	1290	3	1.220	1.69

Concluding remarks

This report summarises results on investigations of the microstructures and microtextures of pure copper, nickel and aluminium subjected to different deformation processes to high ultimate imposed strains. A comparison of the microstructures, dislocation densities and microhardness values developed in pure Al, Ni and Cu during combinations of different strain paths permits the development of a phenomenological model to describe the microhardness evolution with accumulated strain. The application of this model demonstrates satisfactory agreement for aluminium and copper. However, the experimental observation shows an incomplete saturation in nickel which is not predicted by the model.

Acknowledgements This work was supported by the European Research Council under ERC Grant Agreement No. 267464-SPDMETALS.

References

1. Valiev RZ, Islamgaliev RK, Alexandrov IV (2000) Prog Mater Sci 45:103
2. Valiev RZ, Langdon TG (2006) Prog Mater Sci 51:881
3. Zhilyaev AP, Langdon TG (2008) Prog Mater Sci 53:893
4. Zhu YT, Lowe TC, Langdon TG (2004) Scripta Mater 51:825
5. Wilde G, Ribbe J, Reglitz G, Wegner M, Rösner H, Estrin Yu, Zehetbauer M, Setman D, Divinski S (2010) Adv Eng Mater 12:758
6. Gleiter H (2000) Acta Mater 48:1
7. Zhilyaev AP, Gimazov AA, Raab G, Langdon TG (2008) Mater Sci Eng, A 486:123
8. Zhilyaev AP, Gimazov AA, Soshnikova EP, Révész A, Langdon TG (2008) Mater Sci Eng A489:207
9. Iwahashi Y, Horita Z, Nemoto M, Langdon TG (1998) Acta Mater 46:3317
10. Liao XZ, Kilmametov AR, Valiev RZ, Gao H, Li X, Mukherjee AK, Bingert JF, Zhu YT (2006) Appl Phys Lett 88:021909
11. Rajulapati KV, Scattergood RO, Murty KL, Duscher G, Koch CC (2006) Scripta Mater 55:155
12. Rajulapati KV, Scattergood RO, Murty KL, Horita Z, Langdon TG, Koch CC (2008) Metall Mater Trans A 39A:2528
13. Raab GI (2005) Mater Sci Eng A410–411:230
14. Zhilyaev AP, Lee S, Nurislamova GV, Valiev RZ, Langdon TG (2001) Scripta Mater 44:2753
15. Zhilyaev AP, Nurislamova GV, Kim BK, Baró MD, Szpunar JA, Langdon TG (2003) Acta Mater 51:753
16. Oh-ishi K, Zhilyaev AP, McNelley TR (2005) Mater Sci Eng A410–411:183
17. Zhilyaev AP, Oh-ishi K, Langdon TG, McNelley TR (2005) Mater Sci Eng A410–411:277
18. Zhilyaev AP, Oh-ishi K, Raab GI, McNelley TR (2006) Mater Sci Eng A441:245
19. www.ing.unitn.it/∼maud
20. Lutterotti L, Scardi P (1990) J Appl Cryst 23:246
21. Edalati K, Horita K (2011) Acta Mater 59:6831
22. Zhilyaev AP, Swaminathan S, Gimazov AA, McNelley TR, Langdon TG (2008) J Mater Sci 43:7451. doi:10.1007/s10853-008-2714-y
23. Mohamed FA, Dheda SS (2012) Mater Sci Eng A558:59
24. Zhao YH, Liao XZ, Zhu YT, Horita Z, Langdon TG (2005) Mater Sci Eng, A 410–411:188
25. Balogh L, Ungár T, Zhao Y, Zhu YT, Horita Z, Xu C, Langdon TG (2008) Acta Mater 56:809
26. Zhao YH, Horita Z, Langdon TG, Zhu YT (2008) Mater Sci Eng, A 474:342
27. An XH, Lin QY, Wu SD, Zhang ZF, Figueiredo RB, Gao N, Langdon TG (2011) Scripta Mater 64:954
28. Hegedűs Z, Gubicza J, Kawasaki M, Chinh NQ, Fogarassy Z, Langdon TG (2012) J Alloys Comp 536:S190
29. Mazilkin AA, Straumal BB, Borodachenkova MV, Valiev RZ, Kogtenkova OA, Baretzky B (2012) Mater Lett 84:63
30. Chinh NQ, Horváth G, Horita Z, Langdon TG (2004) Acta Mater 52:3555
31. Gubicza J, Chinh NQ, Csanádi T, Langdon TG, Ungár T (2007) Mater Sci Eng A462:86
32. Voce E (1948) J Inst Metals 74:537
33. Zhilyaev AP, Langdon TG (2012) J Mater Sci 47:7888. doi:10.1007/s10853-012-6429-8